Anthropomorphizing the Mouse Cardiac Action Potential via a Novel Dynamic Clamp Method

Rebecca C. Ahrens-Nicklas[†‡] and David J. Christini[†‡*]
[†]Greenberg Division of Cardiology and [‡]Department of Physiology, Biophysics and Systems Biology, Weill Cornell Medical College, New York, New York

ABSTRACT Interspecies differences can limit the translational value of excitable cells isolated from model organisms. It can be difficult to extrapolate from a drug- or mutation-induced phenotype in mice to human pathophysiology because mouse and human cardiac electrodynamics differ greatly. We present a hybrid computational-experimental technique, the cell-type transforming clamp, which is designed to overcome such differences by using a calculated compensatory current to convert the macroscopic electrical behavior of an isolated cell into that of a different cell type. We demonstrate the technique's utility by evaluating drug arrhythmogenicity in murine cardiomyocytes that are transformed to behave like human myocytes. Whereas we use the cell-type transforming clamp in this work to convert between mouse and human electrodynamics, the technique could be adapted to convert between the action potential morphologies of any two cell types of interest.

INTRODUCTION

The electrophysiology of both neurons and cardiac myocytes varies, often significantly, between species due to differences in the expression levels and subtypes of ion channels and transporters. These differences can obscure extrapolation from a model organism's phenotype to human pathophysiology, especially in investigations of cardiac arrhythmias.

This problem is particularly acute when trying to translate from mouse to human. Not only does the mouse heart beat ~10 times faster than the human heart, but the murine action potential duration (APD) can be 10 times shorter and is more triangular than that of human myocytes (1). This difference is largely due to mice lacking the calcium-mediated plateau phase that is responsible for sustaining depolarization in human myocytes (2). Because many drugs and mutations exert their proarrhythmic effects during this plateau in humans, arrhythmia studies in mice often yield ambiguous results. This is unfortunate given the inherent value of the mouse as a model organism, in large part due to our ability to manipulate the murine genome. To circumvent such limitations, we have developed what to our knowledge is a new technique, the cell-type transforming clamp (CTC), that can convert the electrical behavior of a cell into that of a different cell type in real-time (e.g., it can anthropomorphize a mouse action potential).

Traditional whole-cell patch-clamp electrophysiology investigations of isolated cardiac myocytes cannot fully overcome species differences. In voltage-clamp mode, a predetermined membrane voltage waveform (usually a square wave) is input into a cell and the resultant net membrane current is measured, whereas in current-clamp mode, a current stimulus is injected and the resultant membrane voltage waveform (usually an action potential) is recorded. Action potential clamp is a type of voltage-clamp in which an action-potential waveform is used to clamp a cell's voltage (3). A major limitation of this technique is that the voltage waveform is predetermined (not free-running); therefore, it cannot be used to study the arrhythmogenic effects of a drug or a mutation on the voltage waveform.

The CTC differs from these existing electrophysiology techniques in that it is a dynamic-clamp method. Dynamic-clamp is a closed-loop technique that couples real cells to computational models or other real cells (4). This coupling allows for a dynamic current stimulus that changes in real-time as a function of the measured cell behavior, enabling, for example, the elucidation of arrhythmia mechanisms that are not revealed through standard electrophysiology approaches (5–7).

The CTC inserts a computationally calculated virtual conductance into a mouse myocyte to compensate for the differences between mouse and human currents. The value of this technique, as we will demonstrate, is that it allows the mouse myocyte to undergo humanlike membrane potential dynamics in the current-clamp electrophysiology mode. Therefore, unlike in action-potential clamp-mode studies, realistic drug-induced membrane potential perturbations (such as action potential prolongation) can occur, thereby enabling illumination of relevant proarrhythmic effects.

METHODS

The CTC simultaneously couples a target mouse myocyte to a target-canceling (mouse) computational model and a recipient (e.g., human or guinea pig) computational model in a closed-loop circuit (Fig. 1), transforming the membrane potential of the target myocyte to that of a human (or guinea pig). In essence, the drug-induced current from the target myocyte is inserted as an artificial conductance into the recipient model in real-time, thereby revealing the effects of the drug in the context of a humanlike waveform.

Submitted July 10, 2009, and accepted for publication September 1, 2009.

*Correspondence: dchristi@med.cornell.edu

Editor: Dorothy A. Hanck.

0006-3495/09/11/2684/9 $2.00

doi: 10.1016/j.bpj.2009.09.002

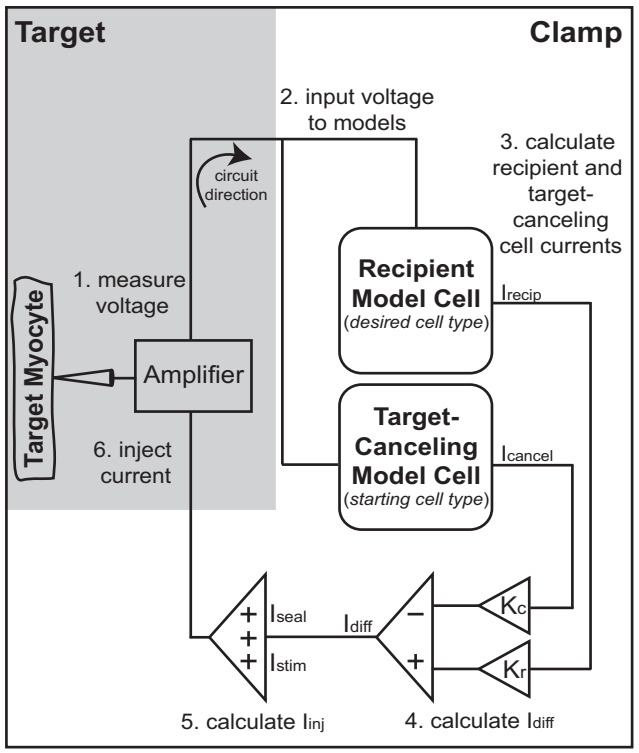

FIGURE 1 Cell-type transforming clamp circuit. An isolated target myocyte is coupled to two computational models (the recipient model cell is the desired cell type, whereas the target-canceling model cell is the same cell type as the target cell). The target cell voltage is measured (step *1*) and input to the recipient and target-canceling models (step *2*). Each model cell current is calculated and scaled by the ratio of the target cell capacitance to the model cell capacitance (K_c and K_r) (step *3*). A difference current, I_{diff}, is calculated by subtracting the scaled target-canceling model current from the scaled recipient model current (step *4*). A stimulus current (I_{stim}) and a current to compensate for leak through the patch-clamp seal (I_{seal}) are added to the difference current to produce the injected current (I_{inj}) (step *5*), which is injected into the target cell (step *6*). The circuit is traversed in real time (at a rate of 10 kHz) to convert the target cell waveform to that of the desired cell type. The experimental (target) portion of the circuit is shaded in gray, whereas the computational (clamp) part of the circuit is white.

First, membrane voltage is measured in the target myocyte and input into both the recipient (humanlike) and target-canceling (mouse) model cells. The ionic currents that occur in response to this voltage are computed in both models and scaled to compensate for cell capacitance differences. A difference current is calculated by subtracting the target-canceling model current from the recipient-model current and is injected (along with any stimulus current and patch seal-leak compensation current) into the cell. In so doing, the circuit inserts a virtual conductance that compensates for the difference between mouse and recipient cell conductances at the measured voltage. The myocyte responds to the injected current such that the membrane voltage will now reflect the virtually inserted difference conductance. The cycle is repeated with an update frequency of 10 kHz.

Circuit design

The target myocyte is bidirectionally coupled to both a recipient model cell (a model of the desired cell type) and the target-canceling model cell (a model of the native isolated cell) as shown in the circuit of Fig. 1. First, consider an untreated target cell. The total target myocyte current, $I_{target}(t)$, is described by the following equations,

$$I_{target}(t) = I_{target,ionic}(t) + I_{inj}(t), \quad (1)$$

$$I_{inj}(t) = I_{diff}(t) + I_{stim}(t) + I_{seal}(t), \quad (2)$$

$$I_{diff}(t) = K_r I_{recip}(t) - K_c I_{cancel}(t), \quad (3)$$

$$I_{seal}(t) = \frac{V_{target}}{R_{seal}}, \quad (4)$$

where $I_{target,ionic}(t)$ is the current through target cell channels, pumps, and exchangers and $I_{inj}(t)$ is the current injected into the target cell. $I_{inj}(t)$ is the sum of the difference current, $I_{diff}(t)$, $I_{stim}(t)$, a square-pulse stimulus current used to trigger action potentials, and $I_{seal}(t)$, a current used to offset any leak through the patch-clamp seal. $I_{diff}(t)$ is calculated using $I_{recip}(t)$ and $I_{cancel}(t)$, the currents computed by the recipient and target-canceling models, respectively. $I_{recip}(t)$ and $I_{cancel}(t)$ are each scaled by a term (K_r and K_c, respectively), where $K_r = C_{M,target}/C_{M,recip}$ (and where $C_{M,target}$ is the measured capacitance of the target cell and $C_{M,recip}$ is the recipient model cell capacitance), and $K_c = C_{M,target}/C_{M,cancel}$ (where $C_{M,cancel}$ is the target-canceling model cell capacitance). $I_{seal}(t)$ is calculated using the voltage of the target cell, V_{target}, and the value of the patch-clamp seal resistance, R_{seal}. In the experiments for this article, R_{seal} is high, thus $I_{seal}(t)$ is small. Nevertheless, for very small cells, even a small leak current through the seal can significantly affect voltage (see Fig. S1 in the Supporting Material). $I_{seal}(t)$ corrects for this artifact.

Substituting Eqs. 2 and 3 into Eq. 1 and using $I = C_M\,dV/dt$ and the values for K_r and K_c gives the equation (note that $I_{stim}(t)$ and $I_{seal}(t)$ are set to 0 from here on for clarity, as stimulus and seal leak currents do not affect the circuit analysis):

$$C_{M,target}\frac{dV_{target}}{dt} = \left[C_{M,target}\frac{dV_{target,ionic}}{dt}\right] + \left[\frac{C_{M,target}}{C_{M,recip}}C_{M,recip}\frac{dV_{recip}}{dt}\right] - \left[\frac{C_{M,target}}{C_{M,cancel}}C_{M,cancel}\frac{dV_{cancel}}{dt}\right], \quad (5)$$

$$\frac{dV_{target}}{dt} = \frac{dV_{target,ionic}}{dt} + \frac{dV_{recip}}{dt} - \frac{dV_{cancel}}{dt}. \quad (6)$$

If the target-canceling computational model perfectly models the target cell (we analyze the realistic situation where the model is imperfect later in Fig. 6), then $dV_{target,ionic}/dt = dV_{cancel}/dt$, which gives

$$\frac{dV_{target}}{dt} = \frac{dV_{recip}}{dt}, \quad (7)$$

i.e., the total voltage change experienced by the target cell is equal to the voltage change of the recipient model cell. If the recipient cell is a human model cell, this would produce a human action potential waveform in the target cell.

Next, consider the case where the target cell is drug-treated; i.e., the case for which the CTC is designed. In this case, Eq. 1 becomes

$$I_{target}(t) = I_{target,ionic}(t) + I_{target,drug}(t) + I_{inj}(t), \quad (8)$$

where $I_{target,drug}(t)$ is the drug-induced current difference between an untreated target cell and a drug-treated target cell. Following the same steps as above (Eqs. 5–7), and if (as above) $dV_{target,ionic}/dt = dV_{cancel}/dt$, then

$$\frac{dV_{target}}{dt} = \frac{dV_{recip}}{dt} + \frac{dV_{target,drug}}{dt}, \quad (9)$$

i.e., if the target-canceling computational model voltage change matches the voltage change due to wild-type (not drug-treated) target cell conductances, then the total voltage change in the drug-treated target cell will be the sum of voltage change in the recipient cell and the voltage change due to the drug-induced current in the target cell.

Importantly, model computations and current clamping of the target cell must be accomplished in near real time. We accomplish this using RTXI (www.rtxi.org), a real-time Linux-based experimental control software system developed in our laboratory (8,9). If this is accomplished, the voltage of the target cell will reveal any differences between the target mouse cell and the target-canceling mouse model cell (i.e., drug-induced differences) in the context of its humanlike action potential waveform.

Computational models used for in silico studies

For the modeling studies presented in this article, a computational model of a neonatal mouse ventricular myocyte was used for both the target myocyte and the target-canceling mouse model cell in the CTC. The same model, which was developed by Wang and Sobie (10), was used for both cells in the circuit. For modeling studies of I_{Kr} block, the target-cell conductance through the I_{Kr} channels was reduced by 10%. For numerical integration of the mouse model equations, an implicit fourth-order Runge-Kutta solver (GNU Scientific Library, www.gnu.org/software/gsl/) was used with a time step of 0.01 ms. Action potentials were triggered in the target cell with a suprathreshold (100 μA/μF) stimulus of 0.5-ms duration.

For the CTC recipient model cell, we chose the Luo-Rudy II (LRII) mid-myocardial guinea pig ventricular myocyte model (11) updated by Faber and Rudy in 2000 (12) as the recipient model for our studies. Although this model is not a human type, we chose it, in part, because it demonstrates the ability of the CTC to reveal rich plateau-stage dynamics such as EADs (13,14). In silico investigations of human models—the reduced (15) (Fig. S2) and full (16) (results not shown) Ten Tusscher models—demonstrated effective wild-type anthropomorphization, but no EADs in response to an LQT3 mutant sodium current that did evoke EADs in an LRII CTC study (results not shown).

Computational models used for in vitro studies

The Wang-Sobie model could not be used for the experimental CTC studies, because it is too computationally intensive for the required 10 kHz circuit rate. Therefore, for the target-canceling model in experiments we used a model of adult mouse cardiomyocyte sarcolemmal currents developed by Pandit et al. (17) and modified by Tranquillo et al. (18) that we modified as described below and in Fig. S3.

Before the start of experiments, we repeated our in silico modeling studies using the modified Pandit model as both the target and target-canceling cells (Fig. S4). The Pandit circuit produced results similar to those seen using the Wang and Sobie circuit. However, because the Pandit model does not have a current formulation for I_{Kr}, the effects of I_{Kr} blockade in a Pandit target cell could not be investigated; therefore, a different repolarizing potassium current ($I_{K,slow}$) was reduced by 30% in Pandit modeling studies of channel blockade (Fig. S4, *c–f*).

There can be significant intermyocyte APD variation. However, for effective CTC performance, mismatch between the target cell and the target-canceling model cell must be minimized. To minimize mismatch, we created a suite of nine candidate neonatal models by modifying the standard Pandit model (see Fig. S2). The nine models varied in APD by 10-ms increments from 20 ms to 100 ms. Before the start of each experiment, the cell was stimulated at a rate of 1 kHz for at least 20 beats to allow action potentials to become stable. Then, the isolated neonatal myocyte was stimulated for 10 beats, from which the average APD was computed. The most appropriate target-canceling model to use for that specific cell was automatically selected from the suite of nine candidate models, as that whose APD was closest to the cell's average APD. To determine which of the nine Pandit models should be used as the target-canceling model in drug studies (the target-canceling model is always untreated, see Eqs. 8 and 9), we calculated the mean APD of all untreated cells examined from a given isolation and used the model with the APD closest to this mean for all drug studies of cells from the same isolation.

The recipient model cell was the same LRII model that was used in the modeling studies. For numerical integration of the model equations, we used a forward Euler scheme with a time step of 0.1 ms. Before the start of experiments, both the recipient and target-canceling models were paced at a rate of 1 Hz (the rate used in experiments) until reaching steady-state APD values (300 s for the LRII, 100 s for the modified Pandit model).

Neonatal cardiac myocyte isolation

All procedures were done in accordance with Weill Cornell Institutional Animal Care and Use Committee regulations. Single ventricular myocytes were isolated from day-1 mouse pups. Neonatal mice were chosen because they express cardiac I_{Kr} channels, which are essential for investigation of I_{Kr} blocking drugs (19). Mice were anesthetized via inhalation of isoflurane, and their hearts were removed and placed into ice-cold Ca^{2+} and Mg^{2+}-free Hank's Balanced Salt Solution. Hearts from one litter of pups were pooled, minced, and transferred into a solution of 25 mg/mL collagenase (Worthington Type II) in Hank's Balanced Salt Solution. The tissue was incubated for 40 min in a shaking 37°C incubator, triturated, and filtered through a cell strainer. The cells were centrifuged at 100 $\times$ *g* for 5 min and resuspended in growth media (DMEM + 10% fetal bovine serum + Primocin (0.1 mg/mL, Invitrogen, Carlsbad, CA)). Cells were preplated for 45 min at 37°C to reduce the number of fibroblasts in the final cultures. After preplating, cells were plated in tissue-culture treated dishes at a final concentration of 1.0 $\times$ 10^5 cells/mL to ensure the presence of isolated cells. Cells were kept at 37°C in a 5% CO_2 incubator and used for electrophysiology studies on the second day after culture.

Electrophysiology

Whole-cell current-clamp recordings were performed at room temperature (21°–24°C). Cells were superfused with a Tyrode's solution containing (in mM): NaCl 140, KCl 4, glucose 5.5, $MgCl_2$1, $CaCl_2$ 1, and HEPES 10. Pipette solution contained (in mM): KCl 110, Na_2ATP 5, EGTA 0.05, HEPES 10, $MgCl_2$1, and $CaCl_2$ 0.025. Pipettes pulled from 1.5-mm glass capillary tubes (Sutter Instrument, Novato, CA) had a final resistance of 3–5 MΩ in solution, and offset potentials were measured and corrected. For studies of I_{Kr} block, 1 μM E-4031 (Sigma, St. Louis, MO) was added to the extracellular solution.

Recordings were performed using RTXI (www.rtxi.org) and an A-M Systems (Sequim, WA) model 2400 patch-clamp amplifier. Cell capacitance was measured in voltage-clamp mode before beginning current clamp studies by adjusting amplifier whole-cell compensation knobs (which measure access resistance and membrane capacitance) to minimize transients resulting from application of a 10 mV square wave of 10-ms duration. Capacitances averaged 19.7 $\pm$ 1 pF (mean $\pm$ SE). The capacitance values were used in conjunction with model cell capacitance values to scale the CTC currents (see Eq. 3). Bridge balance was used to compensate for the voltage drop across the access resistance, which averaged 9.5 $\pm$ 0.4 MΩ. The CTC computational models were solved at a rate of 10 kHz.

Patch seal resistance was measured in voltage-clamp mode (by measuring the current in response to a 10 mV square wave from a holding potential of −80 mV) at the beginning of each experiment and used to calculate $I_{seal}(t)$ throughout the experiments. Seal resistances were 2.1 $\pm$ 0.6 GΩ. Often when the measured R_{seal} was used to calculate $I_{seal}(t)$, the resting membrane voltage became hyperpolarized due to overcompensation. Therefore for each individual cell, the seal resistance value used to calculate $I_{seal}(t)$ was adjusted (reduced to 73 $\pm$ 10% of its measured value) until resting membrane voltage = −80 mV.

Action potentials were evoked at a rate of 1 Hz using depolarizing stimuli 1-ms in duration and 150% of threshold in amplitude. APDs were measured from the time of onset of the upstroke to the time when the potential returned

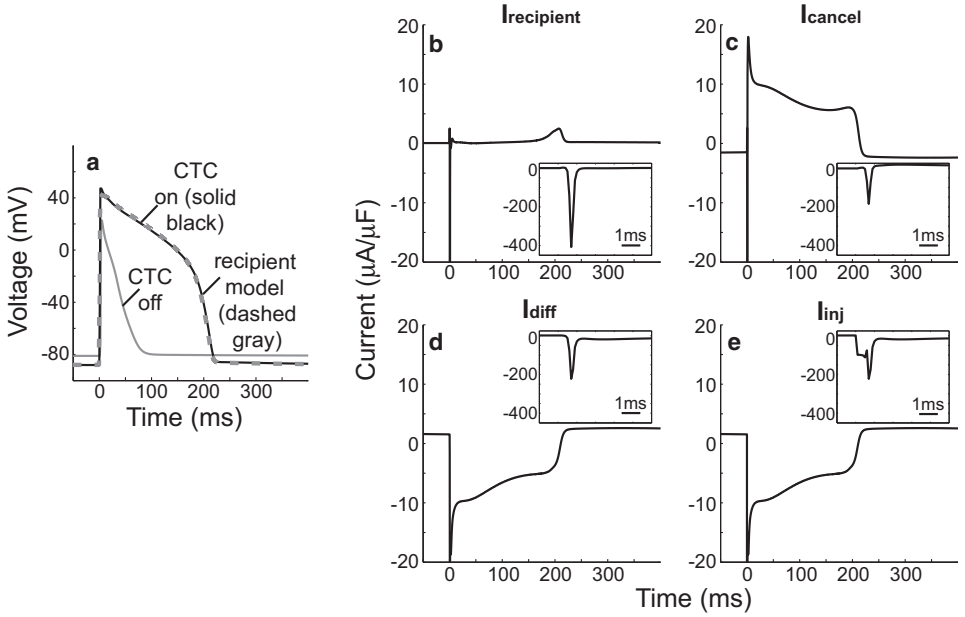

FIGURE 2 CTC can make the waveform of a neonatal mouse model cardiomyocyte humanlike in silico. The CTC was used to clamp an untreated neonatal mouse cardiac myocyte computational model cell (*a*). The CTC prolonged the short action potential of the unclamped cell (*solid gray* versus *black traces*) and induced a phase-3 plateau. The cells were paced at a rate of 1 Hz. The action potential from a statically paced recipient model cell (*a, dashed gray*) is shown for comparison. The currents responsible for the transition are shown (*b–e*). I_{diff} (*d*) is calculated by subtracting I_{cancel} (*c*) from $I_{recipient}$ (*b*). I_{inj} results from the addition of a stimulus current to I_{diff} (*e*). The insets enlarge the first 6 ms of the action potential to show peak current values.

to 80% of the resting membrane potential. Resting membrane potential was measured every cycle and taken to be the voltage of the cell in the timestep before onset of stimulus current.

Cells with APDs during the CTC clamp that were shorter or longer than 1 standard deviation from the mean were not included in the analysis of drug-treatment studies (7:24 cells). Such outlying APDs during the CTC were most likely an artifact of target cell/target-canceling model cell mismatch (in the drug-treated studies, this mismatch was partially due to the use of an average untreated APD value for model selection as described above).

For each experiment, a cell was paced according to the following protocol: 20 stimuli with the CTC off (20 mouse action potentials), 20 s with CTC on but no stimulus (the voltage equilibrates to the recipient model resting membrane potential, as expected from Eqs. 1–9), and 15 stimuli with the CTC on (15 humanlike action potentials).

RESULTS

The CTC can transform the action potential of a mouse model target cell in silico

We first investigated the technique in silico using the Wang and Sobie computational model of a neonatal ventricular mouse myocyte as the target myocyte (Fig. 2). The CTC converted the short, triangular mouse action potential into that of the recipient, LRII model cell. The CTC both prolonged the APD and induced the expected plateau (similar results were seen when a modified Pandit mouse model was used as both the target and target-canceling models; see Fig. S4). The currents responsible for this transition are also shown in Fig. 2, *b–e*.

The CTC can transform the action potential of a real isolated neonatal mouse myocyte in vitro

We applied the CTC to real isolated neonatal cardiac myocytes. As in the modeling studies, the CTC made the action potential humanlike (Fig. 3). This effect was reversible; the waveform returned to its baseline morphology as soon as the CTC was deactivated. Despite experimental cell-to-cell (Fig. 3, *b* and *c*) variation, all clamped cells demonstrated a prolonged APD and plateau. Cell-to-cell and beat-to-beat variability in repolarization time of isolated guinea pig myocytes has been reported previously (20). CTC-clamped myocytes also demonstrate frequency-dependent APD changes (Fig. 3, *d* and *e*).

Fig. 4 demonstrates the experimental current values used to anthropomorphize the isolated target myocyte shown in Fig. 4 *a* (*black trace*). The voltage waveforms and currents are compared to results from in silico studies using the 80-ms Pandit model as both the target cell and target-canceling cell (Fig. 4, *a–f*, *gray traces*). The black, dashed trace in Fig. 4 *f* shows $I_{seal}(t)$ for the experimental trace. The currents from the in silico and in vitro circuits are very similar, with the largest current differences occurring during the first 50 ms of the action potential (this corresponds to the period of greatest voltage difference, Fig. 4 *b*). This difference could be due to mismatch between the target cell and target-canceling model.

The CTC circuit was traversed at a rate of 10 kHz. The rapid upstroke is most sensitive to errors that result from insufficient circuit rates (8). In the sodium channel dynamic-clamp studies of Bettencourt et al. (8), 10 kHz was found to be the rate cutoff for ensuring fidelity in action potential morphologies. As rates were decreased, errors first appeared in the overshoot of the action potential; errors only appeared in other action potential phases at much lower circuit rates. It is possible that the error seen in the early phase of our experimental traces is partially due to an insufficient circuit rate. Importantly, as technology improves in the future, CTC circuit rate will increase, thereby decreasing circuit rate-induced errors.

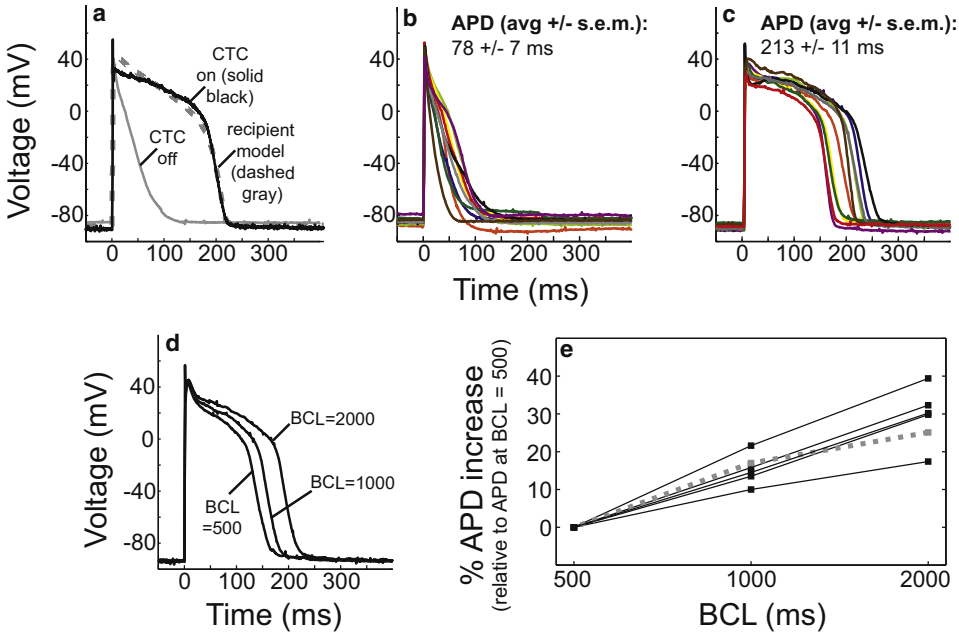

FIGURE 3 CTC can anthropomorphize the action potential of real isolated neonatal mouse myocytes in vitro. The CTC was used to clamp an isolated neonatal mouse myocyte (*a*). The CTC converted the short mouse action potential (*gray*) into that of the recipient model cell (*black*). The action potential from a statically paced recipient model cell (*a, dashed gray*) is shown for comparison. Results from 10 different cells without clamping (*b*) and during clamping (*c*) are shown (*traces* of the *same color* in *b* and *c* correspond to the same cell). Cells were stimulated at 1 Hz. In panels *d* and *e* after 20 s with the CTC on in the absence of pacing, cells were stimulated for 20 cycles at 2 Hz, followed by 20 cycles at 1 Hz, and finally 20 cycles at 0.5 Hz. Representative rate-dependent action potential morphologies from one cell are shown (*d*). Rate-dependent percentage changes in the mean APD for five cells are shown (*e*). The APD response of the recipient model is shown (*e, dotted gray*).

The CTC can be used to assess the arrhythmogenic potential of an I_{Kr}-blocking drug in silico

Importantly, the CTC can be used to investigate drug or mutation-induced arrhythmias, to augment existing preclinical drug safety screens (21) or to assess phenotypes of genetically engineered mouse models of inherited arrhythmia syndromes. Many potential drugs produce proarrhythmic off-target blockade of the repolarizing rapid delayed rectifier cardiac potassium current (I_{Kr}) channel (22), which is the major repolarizing current during the late phase of the human cardiac action potential. I_{Kr} blockade causes APD prolongation and can lead to drug-induced long QT syndrome, a condition that can induce ventricular fibrillation and death. During the short action potential of the unclamped mouse cell, I_{Kr} is not the major repolarizing current (23); thus, unclamped cells are ill-suited for revealing drug proarrhythmia. In contrast, in CTC-clamped cells, I_{Kr} has more time to activate and contribute to the dynamics of the late phase of the action potential, as in human myocytes. Therefore, the effects of drugs that block I_{Kr} can be unmasked through use of the CTC.

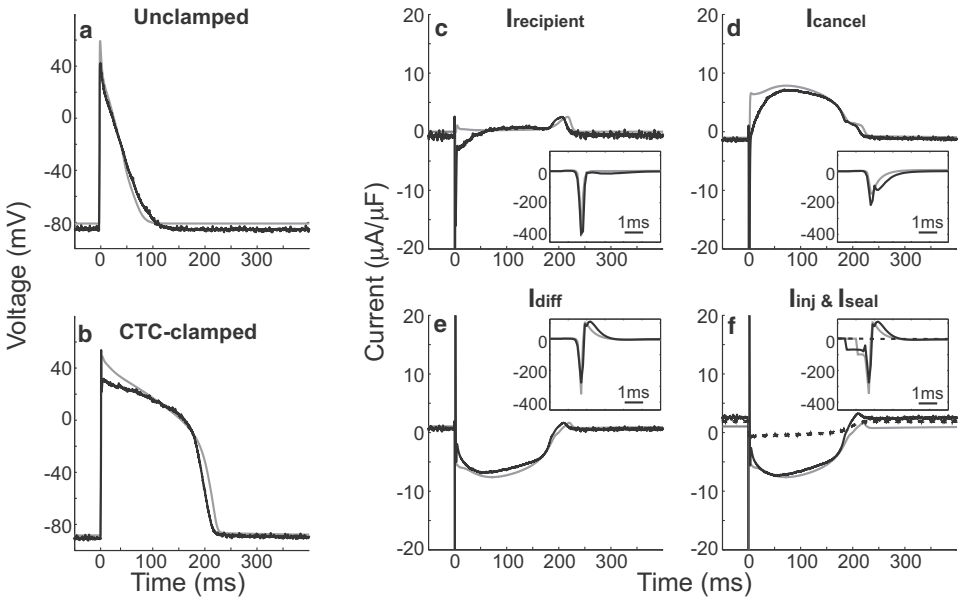

FIGURE 4 In silico and in vitro CTC circuits use similar currents to anthropomorphize a target cell. Traces from in vitro (*black*) and in silico CTC circuits (*gray*) are shown. In the in silico circuit, the 80-ms modified Pandit model was used as both the target cell and target-canceling model. Under both unclamped (*a*) and clamped (*b*) conditions, the model and real experimental voltages are similar. $I_{recipient}$ (*c*), I_{cancel} (*d*), I_{diff} (*e*), and I_{inj} (*f*) from both the in silico and in vitro studies are shown. The insets enlarge the first 6 ms of the action potential to show peak current values. The dashed black line of panel *f* shows the experimental I_{seal}. Cells were stimulated at 1 Hz. The model cell stimulus was 0.5 ms in duration and 100 μA/μF in magnitude. The experimental cell stimulus was 150% of threshold, 1 ms in duration and 71 μA/μF in magnitude.

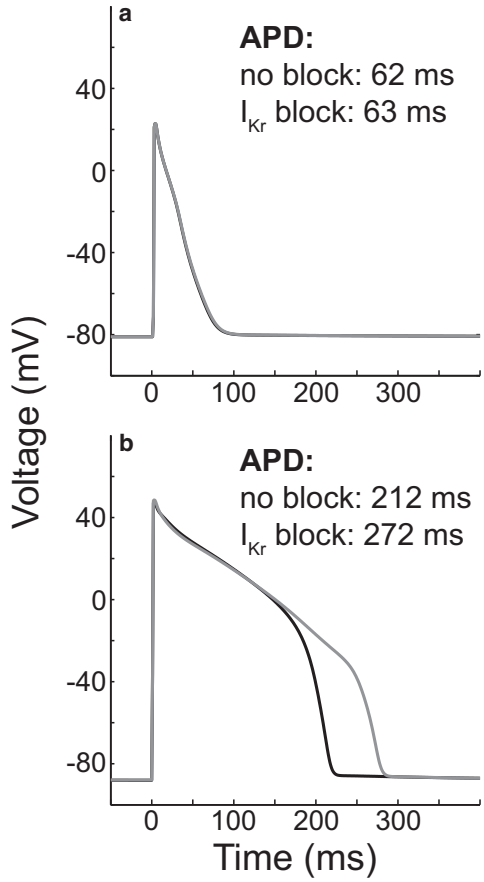

FIGURE 5 CTC reveals the arrhythmogenic potential of I_{Kr}-blockade in silico. Model cells in the presence of I_{Kr}-blockade (*gray traces*) demonstrated longer action potentials relative to cells without I_{Kr} block (*black traces*) only during CTC-clamping (*b* versus *a*). Cells were stimulated at 1 Hz.

The effects of the I_{Kr}-blockade on neonatal mouse cardiac myocytes were assessed in silico (Fig. 5). I_{Kr}-blockade was modeled by decreasing the conductance through the I_{Kr} channel by 10%. In modeling studies, I_{Kr}-blockade had little effect on an unclamped cell (Fig. 5 *a*), yet substantially prolonged the APD in a CTC-clamped cell (Fig. 5 *b*). Ten-percent reduction was chosen because it prolonged the APD during CTC-clamping to a similar degree as seen in studies of isolated guinea pig myocytes treated with 5 μM E-4031 (24). In the studies of Sanguinetti et al. (24), E-4031 prolonged the guinea pig APD from 212 to 268 ms at physiological temperatures, whereas in our in silico CTC studies 10% I_{Kr} blockade prolonged the APD from 212 to 272 ms.

Even in the presence of target/target-canceling cell mismatch drug-induced phenotypes are uncovered by the CTC in silico

The traces from Fig. 5 demonstrate an ideal CTC for which the untreated target cell and the target-canceling model cell are identical. However, in experimental studies the target-canceling model cell never exactly matches the target cell. We studied the influence that this difference would have on the ability of the CTC to detect drug-induced effects. We used a Monte Carlo method to perturb our target cell model so that it would differ from the target-canceling model cell, thereby simulating real cell-to-cell variability as well as model mismatch. Each of the 12 Wang and Sobie mouse-model target cell conductance values were perturbed by a percentage selected from a normal distribution (mean 0, standard deviation 5%). Twenty unique target cell models were created. Untreated and I_{Kr}-blockade model variants were created from the same 20 parameter combinations, differing only in the presence of full or 90% I_{Kr} conductance.

Action potentials from each of the perturbed mouse models are shown in Fig. 6, *a* and *c*. The APD_{90} of the untreated models was 62 $\pm$ 0.2 ms (mean $\pm$ SE), and the APD_{90} of the I_{Kr}-blockade models was 63 $\pm$ 0.2 ms. When these 20 model target cells were placed in the CTC, they recapitulated qualitatively the results seen when an ideal target cell was used. All 20 models showed action potential prolongation relative to untreated when they had I_{Kr}-blockade and the CTC was turned on (Fig. 6, part *d* versus part *b*). Six out of 20 of the CTC-clamped I_{Kr}-blockade models had EADs (which were not seen when an ideal target cell was used). This suggests that mismatch between the target cell and the target-canceling cell can lead to an overestimation of the severity of the drug-induced phenotype. In studies of real isolated myocytes, traces with action potential durations that were substantially greater or less than the mean APD (i.e., >1 SD different) were not included in the analysis to minimize these mismatch-induced errors.

The CTC unmasks drug-induced arrhythmogenicity of the IKr-blocking drug E-4031 in isolated neonatal murine cardiac myocytes

In real isolated myocytes, 1 μM E-4031 prolonged the APD of unclamped cells as compared to untreated cells (118 $\pm$ 14 ms, $n = 7$ vs. 78 $\pm$ 7 ms, $n = 10$ (mean $\pm$ SE)) (Fig. 7 *a*). However, the amount of prolongation in CTC-clamped cells was greater (Fig. 7 *b*). E-4031-treated CTC-clamped cells had an average APD of 298 $\pm$ 25 ms, whereas untreated cells averaged 213 $\pm$ 11 ms. E-4031 prolonged the action potential of clamped cells by 85 ms, while prolonging the APD of nonclamped cells 40 ms.

Importantly, only clamped cells demonstrated a plateau, which is essential for many of the arrhythmogenic sequellae of action potential prolongation (25). Therefore, as predicted by the modeling studies of Fig. 6, in spite of target/target-canceling cell mismatch, the proarrhythmic effects of E-4031 are evident in CTC-clamped mouse cells.

As described above, previously published studies of guinea pig myocytes treated with 5 μM E-4031 (24) demonstrated prolongation of the APD from 212 to 268 ms (24). Our 1 μM E-4031 treated CTC-clamped isolated neonatal

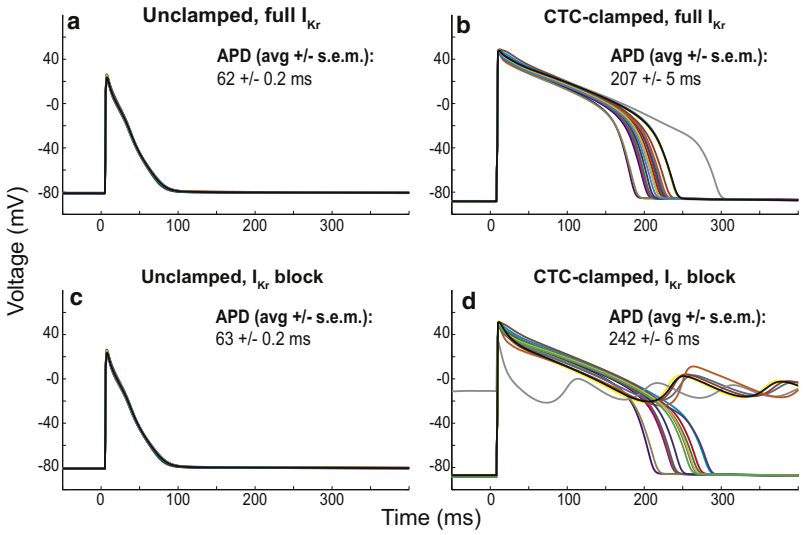

FIGURE 6 CTC-clamped I_{Kr}-blocked myocytes accurately demonstrate drug-induced APD prolongation even in the presence of mismatch between the target and target-canceling model cell in silico. Twenty wild-type and I_{Kr}-blocked model variants were created. The original unperturbed Wang and Sobie model was the target-canceling model; therefore, there was mismatch between the target and target-canceling cell in each case. Traces of the same color in panels *a–d* represent results from the same model variant. In the unclamped cell, there was no major difference between the APDs of blocked and unblocked cells (*a* versus *c*). However, in the CTC-clamped models, even in the presence of cell-to-cell variation, the APD-prolonging effects of I_{Kr}-block were seen in every model (*b* versus *d*). Mismatch between the target and target-canceling cell led to EADs in six out of the 20 models tested. These six traces are examples where model mismatch led to an overestimation of the effects of I_{Kr} block. The measured average APD value in the CTC-clamped I_{Kr}-blocked cells (242 ms) is artificially short because beats with EADs could not be included in the quantification. Cells were stimulated at 1 Hz for 100 unclamped cycles followed by 20 no-stimulus CTC-clamped cycles and 80 stimulated CTC-clamped cycles. In cells with EADs, full repolarization did not occur before the next stimulus and EADs persisted even after 200 additional CTC-clamped cycles.

mouse myocytes demonstrated APD prolongation from 213 to 298 ms (Fig. 7). Some important experimental differences exist between the published guinea pig studies and the study of Fig. 7 including: the guinea pig studies were performed at 35°C and a stimulation rate of 0.5 Hz, whereas our studies were performed at room temperature and a stimulation rate of 1 Hz. In addition, the doses of E-4031 were different (1 μM vs. 5 μM); however, both of these doses produce similar responses in dose-response studies of isolated guinea pig myocytes (24). Despite these experimental differences, both studies demonstrated a similar degree of APD prolongation and absence of EAD formation.

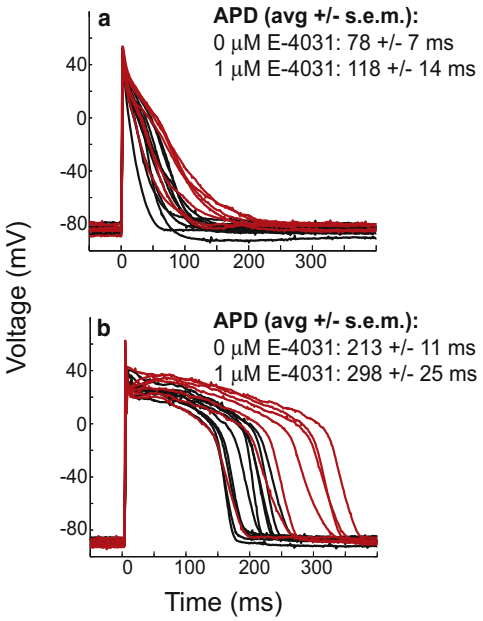

FIGURE 7 CTC reveals the arrhythmogenic potential of the I_{Kr}-blocking drug, E-4031. In real isolated cells, I_{Kr}-blockade by E-4031 prolonged the unclamped action potential (*a, red-treated* ($n = 7$) versus *black-untreated* ($n = 10$), two-tailed unpaired *t*-test, $p = 0.015$). However, in CTC-clamped real myocytes, E-4031-induced prolongation was increased by 45 ms (*b, red-treated* versus *black-untreated*, two-tailed unpaired *t*-test, $p = 0.003$). Cells were stimulated at 1 Hz.

DISCUSSION

Benefits of the CTC

We have demonstrated that the CTC can be used to convert the action potential waveform of a neonatal mouse myocyte into that of a human in real-time. The potential arrhythmogenic effects of drugs can be screened through use of this system. Currently available screening approaches include assessing the propensity of a drug to reduce I_{Kr} current in a heterologous cell line that expresses hERG channels. One limitation of this approach is that the heterologous cell, such as an HEK-293 cell, is not a cardiac myocyte and therefore lacks the full complement of cardiac ion channels and proteins that modulate the function of ion channels. Studies have demonstrated that some compounds that demonstrate hERG-inhibition in heterologous cell system screens are actually safe in real cardiac myocytes and tissues (26). Screens in cardiac myocytes and tissues have proven to be more effective. Although these screens can be done in myocytes from larger animals such as guinea pigs or rabbits, this would significantly increase the cost of the screen. Another important benefit of the CTC is that because of the ability to manipulate the murine genome, CTC studies in mice could be used to investigate genotype-specific drug reactions.

The CTC is limited by the availability of good computational models of the cell types of interest. One potential improvement to the technique would be to automatically

tune the target-canceling model to match the target cell using a method such as a genetic algorithm (27) (as compared to the current approach of selecting one of nine candidate models). Future studies will benefit both from the constant improvements being made to models of excitable cells and from increases in computational power.

Limitations

In this study, all experiments were conducted at room temperature. It is possible that future studies conducted at physiological temperature may require faster circuit rates (>10 kHz) and larger injected currents and therefore may be more technically difficult to perform. In addition, prolonged injection of larger currents could perturb the ionic composition of the cytosol.

The CTC anthropomorphizes the membrane potential; however, it does not compensate for differences between human and mouse intracellular calcium cycling (28). Future calcium imaging studies comparing CTC-clamped mouse myocytes and paced guinea pig myocytes could provide important insights into these differences in calcium dynamics.

Several factors could lead to errors in the circuit, including mismatch between the target cell and target-canceling model. We investigated the effects of this mismatch in Fig. 6 and Fig. S4; however, there could be a greater degree of variation in expression levels of individual channels or cell-to-cell variation in channel kinetics that were not fully captured in our modeling studies. Mismeasurement of target cell capacitance could also be a source of error in the circuit.

We have tried to minimize model mismatch by producing a suite of models that can be used as the target-canceling model. Selection of the proper model for drug-treated studies was determined by results from untreated cells from the same isolation, which likely introduced an error into the circuit. Furthermore, future CTC studies in genetically modified mice may require new approaches to minimizing isolation-to-isolation variability so that the correct target-canceling model from wild-type experiments can be used as the model for mutation experiments. For example, the wild-type and mutant isolations could be done in parallel to ensure that all elements of the culture process (enzymatic digestion times, reagents, etc.) are as similar as possible.

In addition to using a target-canceling model cell, the CTC relies on a humanlike recipient model to anthropomorphize the target cell. Any errors in the recipient model cell are propagated as errors to the circuit itself. Models are created by fitting data that is acquired under specific experimental conditions; therefore, they may not fully capture all cell dynamics if the model is run under conditions far from those used to make the model.

Due to both the complexity of the CTC technique and cell-to-cell variation, a large sample number may be necessary in future studies of subtle phenotypes to obtain statistical significance. In addition, eliminating outlier traces (as we have done in this study) may introduce a bias in the analysis of the data. However, as models and model selection techniques improve to minimize model and target cell mismatch, we believe that the occurrence of outliers will decrease.

In conclusion, the CTC can be used for a wide range of applications. Although we have demonstrated its ability to make mouse cardiac electrodynamics more humanlike, it can be used to reversibly convert between the membrane potentials of any two cell types, whether they are from different species or from different populations of cells within the same organism. All that is required to adapt the technique for different applications are computational models of the appropriate cell types. This technology could also be integrated into existing high-throughput electrophysiology platforms (29) to allow for large-scale screening of human relevant proarrhythmic effects of drug compounds.

SUPPORTING MATERIAL

Four figures are available at http://www.biophysj.org/biophysj/supplemental/S0006-3495(09)01445-3.

We thank Jonathan Bettencourt and Tashalee Brown for technical assistance and Eric Sobie for model code.

This work was supported by National Institutes of Health grants No. 2R01RR020115, MSTP No. GM07739, and fellowship No. 1F30HL094073-01.

REFERENCES

1. Salama, G., and B. London. 2007. Mouse models of long QT syndrome. *J. Physiol.* 578:43–53.
2. Nerbonne, J. M. 2004. Studying cardiac arrhythmias in the mouse—a reasonable model for probing mechanisms? *Trends Cardiovasc. Med.* 14:83–93.
3. Doerr, T., R. Denger, and W. Trautwein. 1989. Calcium currents in single SA nodal cells of the rabbit heart studied with action potential clamp. *Pflugers Arch.* 413:599–603.
4. Wilders, R. 2006. Dynamic clamp: a powerful tool in cardiac electrophysiology. *J. Physiol.* 576:349–359.
5. Berecki, G., J. G. Zegers, A. O. Verkerk, Z. A. Bhuiyan, B. de Jonge, et al. 2005. HERG channel (dys)function revealed by dynamic action potential clamp technique. *Biophys. J.* 88:566–578.
6. Berecki, G., J. G. Zegers, Z. A. Bhuiyan, A. O. Verkerk, R. Wilders, et al. 2006. Long-QT syndrome-related sodium channel mutations probed by the dynamic action potential clamp technique. *J. Physiol.* 570:237–250.
7. Prinz, A. A., L. F. Abbott, and E. Marder. 2004. The dynamic clamp comes of age. *Trends Neurosci.* 27:218–224.
8. Bettencourt, J. C., K. P. Lillis, L. R. Stupin, and J. A. White. 2008. Effects of imperfect dynamic clamp: computational and experimental results. *J. Neurosci. Methods.* 169:282–289.
9. Dorval, A. D., D. J. Christini, and J. A. White. 2001. Real-time LINUX dynamic clamp: a fast and flexible way to construct virtual ion channels in living cells. *Ann. Biomed. Eng.* 29:897–907.
10. Wang, L. J., and E. A. Sobie. 2008. Mathematical model of the neonatal mouse ventricular action potential. *Am. J. Physiol. Heart Circ. Physiol.* 294:H2565–H2575.

11. Luo, C. H., and Y. Rudy. 1994. A dynamic model of the cardiac ventricular action potential. II. Afterdepolarizations, triggered activity, and potentiation. *Circ. Res.* 74:1097–1113.

12. Faber, G. M., and Y. Rudy. 2000. Action potential and contractility changes in $[Na^+]_i$ overloaded cardiac myocytes: a simulation study. *Biophys. J.* 78:2392–2404.

13. Clancy, C. E., and Y. Rudy. 1999. Linking a genetic defect to its cellular phenotype in a cardiac arrhythmia. *Nature.* 400:566–569.

14. Zeng, J., and Y. Rudy. 1995. Early afterdepolarizations in cardiac myocytes: mechanism and rate dependence. *Biophys. J.* 68:949–964.

15. Ten Tusscher, K. H., and A. V. Panfilov. 2006. Cell model for efficient simulation of wave propagation in human ventricular tissue under normal and pathological conditions. *Phys. Med. Biol.* 51:6141–6156.

16. Ten Tusscher, K. H., and A. V. Panfilov. 2006. Alternans and spiral breakup in a human ventricular tissue model. *Am. J. Physiol. Heart Circ. Physiol.* 291:H1088–H1100.

17. Pandit, S. V., R. B. Clark, W. R. Giles, and S. S. Demir. 2001. A mathematical model of action potential heterogeneity in adult rat left ventricular myocytes. *Biophys. J.* 81:3029–3051.

18. Tranquillo, J. V., J. Hlavacek, and C. S. Henriquez. 2005. An integrative model of mouse cardiac electrophysiology from cell to torso. *Europace.* 7 (Suppl 2):56–70.

19. Wang, L., Z. P. Feng, C. S. Kondo, R. S. Sheldon, and H. J. Duff. 1996. Developmental changes in the delayed rectifier K^+ channels in mouse heart. *Circ. Res.* 79:79–85.

20. Zaniboni, M., A. E. Pollard, L. Yang, and K. W. Spitzer. 2000. Beat-to-beat repolarization variability in ventricular myocytes and its suppression by electrical coupling. *Am. J. Physiol. Heart Circ. Physiol.* 278:H677–H687.

21. Gintant, G. A. 2008. Preclinical Torsades-de-Pointes screens: advantages and limitations of surrogate and direct approaches in evaluating proarrhythmic risk. *Pharmacol. Ther.* 119:199–209.

22. Sanguinetti, M. C., and M. Tristani-Firouzi. 2006. hERG potassium channels and cardiac arrhythmia. *Nature.* 440:463–469.

23. Nuss, H. B., and E. Marban. 1994. Electrophysiological properties of neonatal mouse cardiac myocytes in primary culture. *J. Physiol.* 479:265–279.

24. Sanguinetti, M. C., N. K. Jurkiewicz, A. Scott, and P. K. S. Siegl. 1991. Isoproterenol antagonizes prolongation of refractory period by the class III antiarrhythmic agent E-4031 in guinea pig myocytes. *Circ. Res.* 68:77–84.

25. Antzelevitch, C., and W. Shimizu. 2002. Cellular mechanisms underlying the long QT syndrome. *Curr. Opin. Cardiol.* 17:43–51.

26. Dumotier, B. M., M. Deurinck, Y. Yang, M. Traebert, and W. Suter. 2008. Relevance of in vitro SCREENIT results for drug-induced QT interval prolongation in vivo: a database review and analysis. *Pharmacol. Ther.* 119:152–159.

27. Syed, Z., E. Vigmond, S. Nattel, and L. J. Leon. 2005. Atrial cell action potential parameter fitting using genetic algorithms. *Med. Biol. Eng. Comput.* 43:561–571.

28. Bers, D. M., J. W. Bassani, and R. A. Bassani. 1996. Na-Ca exchange and Ca fluxes during contraction and relaxation in mammalian ventricular muscle. *Ann. N. Y. Acad. Sci.* 779:430–442.

29. Dunlop, J., M. Bowlby, R. Peri, D. Vasilyev, and R. Arias. 2008. High-throughput electrophysiology: an emerging paradigm for ion-channel screening and physiology. *Nat. Rev. Drug Discov.* 7:358–368.